The Axisymmetric Contact Problem between a Rigid Spherical Indenter and a Concentrically Rippled Surface

In this section, the numerical simulation for the axisymmetric contact problem between a rigid spherical indenter and a concentrically rippled surface is presented. This particular geometry, as shown in Fig. A1, was chosen for its simplicity and because the analytical solution is known and consequently provides a baseline to compare against. We will compare our numerical results with the analytical results provided by Guduru[10] and Kesari et al.[30], so we here summarize a few of their basic results.

Using the dimensionless parameters $\xi_1 = \pi(9a_3a_2^{-2})^{1/3}$ and $\xi_2 = \pi a_1(a_2a_3^{-2}/3)^{1/3}$ the normal load *f*, separation α and mean contact radius c_c in normalized form (F, Δ, C) are shown to be related as:

$$\Delta \equiv \frac{\alpha R_s}{c_r^2} = C^2 - \frac{2}{3}\sqrt{2C} + \frac{2\xi_1\xi_2 C}{3} H_0(\xi_1 C) \qquad \text{(A1)}$$

$$F \equiv \frac{f}{3\pi R_s W_{ad}} = C^3 - \sqrt{2C^3} + \frac{2}{3\pi}\xi_1^2\xi_2 C^3 + \xi_2 C H_1(\xi_1 C) - \xi_1\xi_2 C^2 H_2(\xi_1 C) \qquad \text{(A2)}$$

where $H_n(.)$ is the Struve function of order *n*, $C \equiv \frac{c_c}{c_r}$, and $c_r \equiv (9a_2a_3)^{1/3} R_s/2 = (9\pi/4)^{1/3}(\varepsilon R_s)^{1/2}\mu^{1/2}$. Note that (A1) and (A2) are only valid for full contact.

The dimensionless energy release rate Γ is found to be

$$\Gamma \equiv \frac{G}{W_{ad}} = \frac{[C^3 + \frac{2}{3\pi}\xi_1^2\xi_2 C^3 + \xi_2 C H_1(\xi_1 C) - \xi_1\xi_2 C^2 H_2(\xi_1 C) - F]^2}{2C^3} \qquad \text{(A3)}$$

In the absence of the ripples (A1) and (A2) get reduced to the solution to the classical JKR solution

$$F = C^3 - \sqrt{2C^3}, \quad \Delta = C^2 - \frac{2}{3}\sqrt{2C} \qquad \text{(A4)}$$

The equilibrium force-displacement curve has oscillations, or folds, owing to the sinusoidal topography of the surfaces, and the envelope of the folded analytic curve is given by Kesari et al.[30] as follows:

$$\Delta = C^2 - \frac{2}{3}\sqrt{2C} \pm \left(\frac{8}{9\pi}\right)^{1/2} \xi_2 \xi_1^{1/2} C^{1/2} \qquad \text{(A5)}$$

$$F = C^3 - \sqrt{2C^3} \pm \left(\frac{2}{\pi}\right)^{1/2} \xi_2 \xi_1^{1/2} C^{3/2} \qquad \text{(A6)}$$

The basic approach to numerically solving this problem is the same as that for solving the non-axisymmetric adhesive contact problem, i.e. (1)-(10b), except that the U_w term is replaced by the following:

$$U_w = -A[1-\cos(KR)] \qquad \text{(A7)}$$

where $R = \sqrt{X^2 + Y^2}$.

First, we simulate the following case: $a_1 = -0.005$, $a_2 = 0.2$, $a_3 = 0.005$ and $\mu = 1.0$, which satisfies the monotonicity condition (12). The rippled surface U_w from (A7) and the initial gap U_0 from (10a) are shown in Fig. A2(a). The normalized force versus normalized displacement is shown in Fig. A2(b). Our numerical results agree very well with Guduru's solution[10], and the pull-off force F_c for the rippled surface is larger than its smooth counterpart where $F_c = 0.5$, resulting in interface strengthening. Fig. A2(c) plots a series of normalized pressure distributions P for $\mu = 1.0$ at *D=-2.0, -1.0, 1.0* and *2.0* during approach and detachment. The corresponding values of $\Delta \equiv (4/9\pi)^{2/3} D/\mu$ are: *-0.54, -0.27, 0.27* and *0.54*, shown as four red points in Fig. A2(b). It shows that two different equilibriums coexist at $\Delta = -0.54$, and this process is not reversible.

We then simulate the following case: $a_1 = 0.004$, $a_2 = 0.02$, $a_3 = 0.03$ and $\mu = 2.2$, which does not satisfy the monotonicity condition (12). The rippled surface U_w and the initial gap U_0 are shown in Fig. A3(a). The normalized force versus displacement is plotted in Fig. A3(b). The pull-off force is slightly increased to $F_c = 0.55$. Although the monotonicity condition (12) is not satisfied, our numerical results agree fairly well with Guduru's solution, because the ripple troughs can spontaneously jump into contact with the indenter, as shown in Fig. A3(c), which plots a series of normalized pressure distributions P at *D=-4.46*, *-3.24* and *-2.03* during approach and detachment. The corresponding values of Δ are shown as three red points in Fig. A3(b).

We finally simulate the following case: $a_1 = 0.08$, $a_2 = 0.007$, $a_3 = 0.025$ and $\mu = 1.6$, which satisfy neither the monotonicity condition (12) nor the jump-to-contact condition (13). The rippled surface U_w and the initial gap U_0 are shown in Fig. A4(a). The normalized force versus displacement is shown in Fig. A4(b), which illustrates how increasing the ripple amplitude makes the corrugations on the force-displacement curve much deeper and closer (hence appearing as lines), indicating that the approach/detachment process proceeds in alternating stable and unstable segments, leading to a greater increase in energy dissipation and the pull-off force compared to the flat surface. However, the numerical simulation results are quite different from Guduru's solution, implying that Guduru's solution is not valid when only partial contacts occur, and the pull-off force is actually decreased, instead of being increased, to a very small value of 0.31.

Figures

A1. Schematic of the axisymmetric adhesive contact between a rigid spherical indenter and a concentrically rippled surface. The amplitude and wavelength have been exaggerated in the diagram for visual clarity. (a) $a < 0$, central concave trough. (b) $a > 0$, central convex asperity.

A2. The axisymmetric adhesive contact between a rigid spherical indenter and a concentrically rippled surface: $a_1 = -0.005$, $a_2 = 0.2$ and $a_3 = 0.005$.

A2(a). The rippled surface U_w and the initial gap U_0.

A2(b). Normalized load F versus normalized displacement Δ.

A2(c). Normalized pressure distributions P for $\mu = 1.0$ at *D=-2.0, -1.0, 1.0* and *2.0* during approach and detachment. The corresponding values of Δ are: *-0.54, -0.27, 0.27* and *0.54*, shown as four red points in Fig. A2(b).

A3. The axisymmetric adhesive contact between a rigid spherical indenter and a concentrically rippled surface: $a_1 = 0.004$, $a_2 = 0.02$ and $a_3 = 0.03$.

A3(a). The rippled surface U_w and the initial gap U_0.

A3(b). Normalized load F versus normalized displacement Δ.

A3(c). Normalized pressure distributions P for $\mu = 2.2$ at *D=-4.46, -3.24* and *-2.03* during approach and detachment. The corresponding values of Δ are shown as three red points in Fig. A3(b).

A4. The axisymmetric adhesive contact between a rigid spherical indenter and a concentrically rippled surface: $a_1 = 0.08$, $a_2 = 0.007$ and $a_3 = 0.025$.

A4(a). The rippled surface U_w and the initial gap U_0.

A4(b). Normalized load F versus normalized displacement Δ.

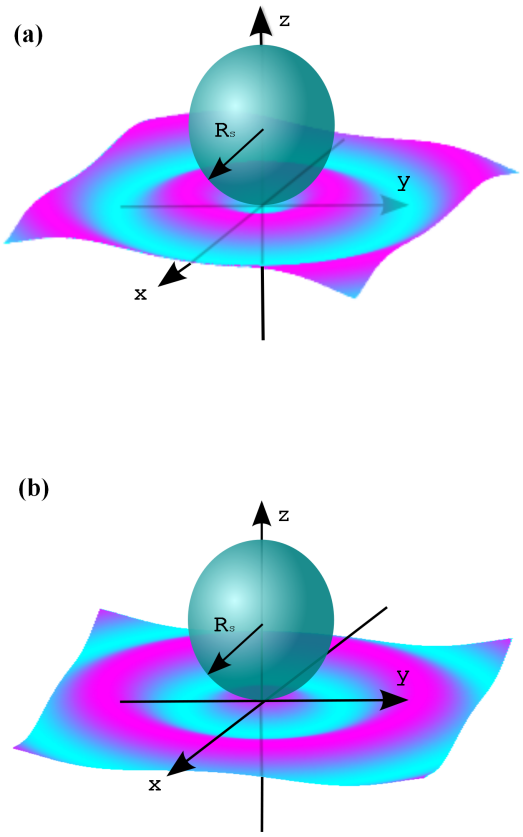

Figure A1

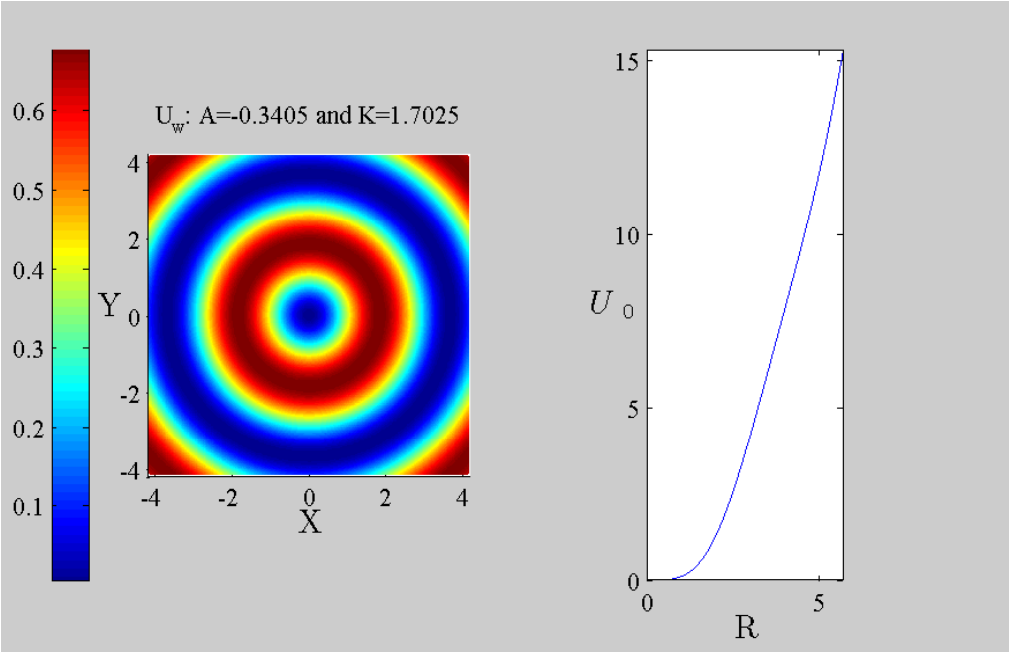

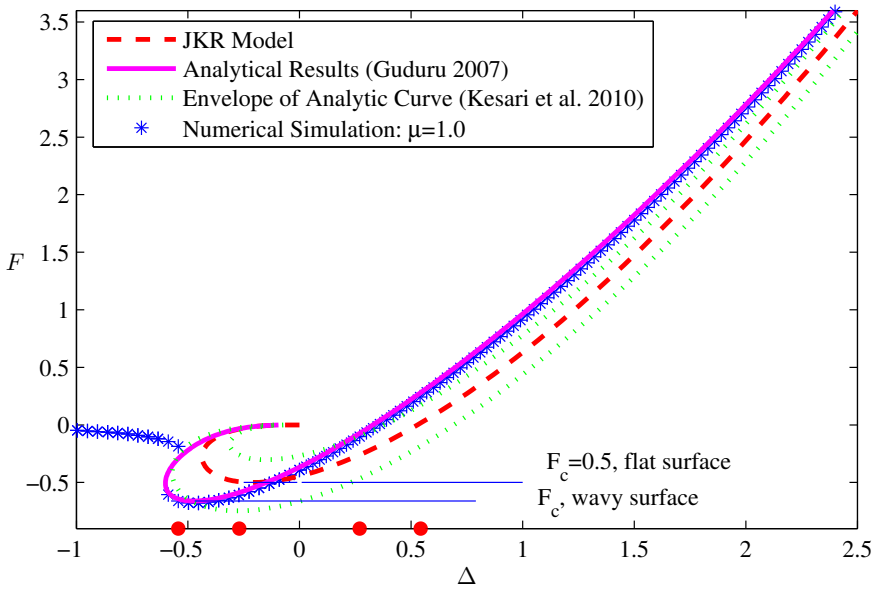

Figure A2

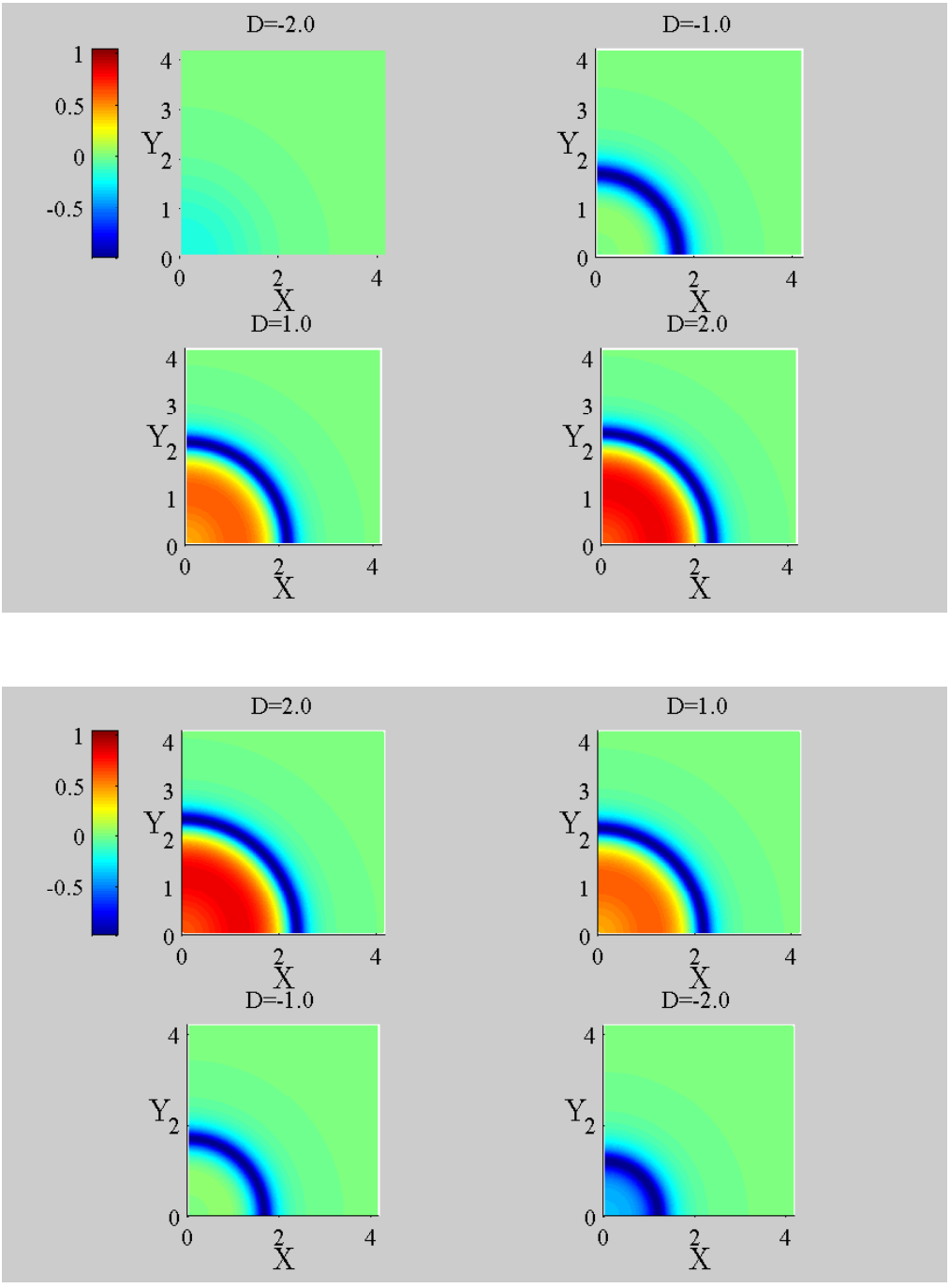

Figure A2

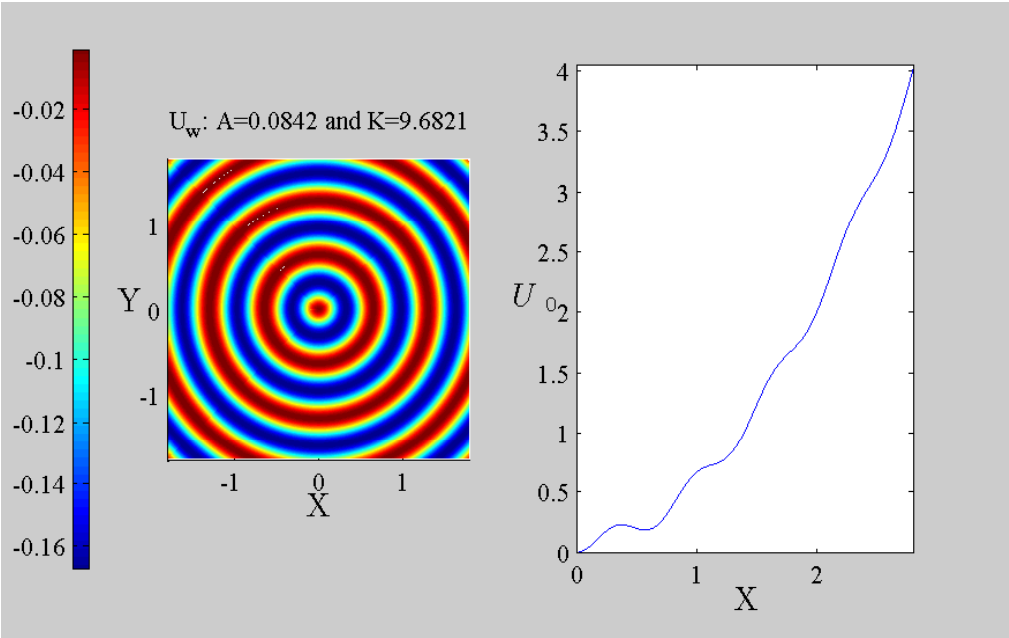

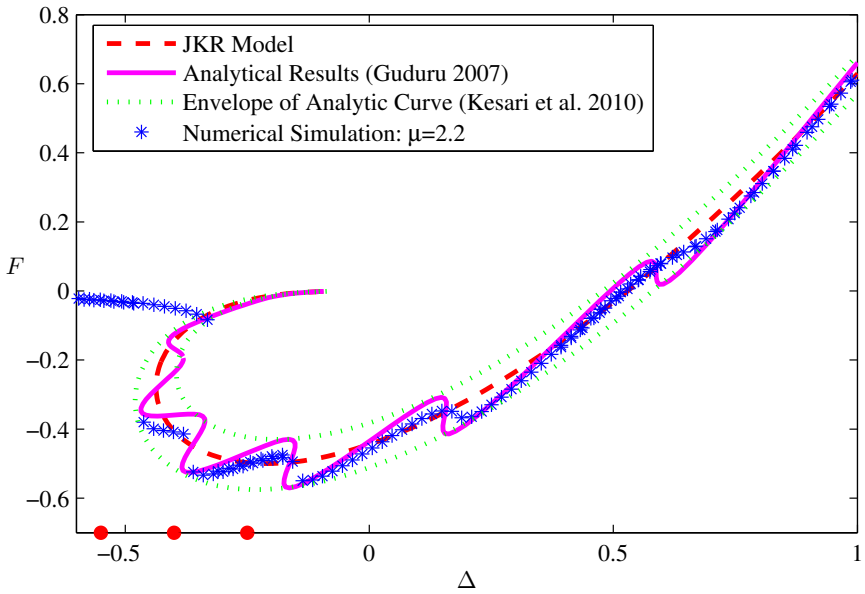

Figure A3

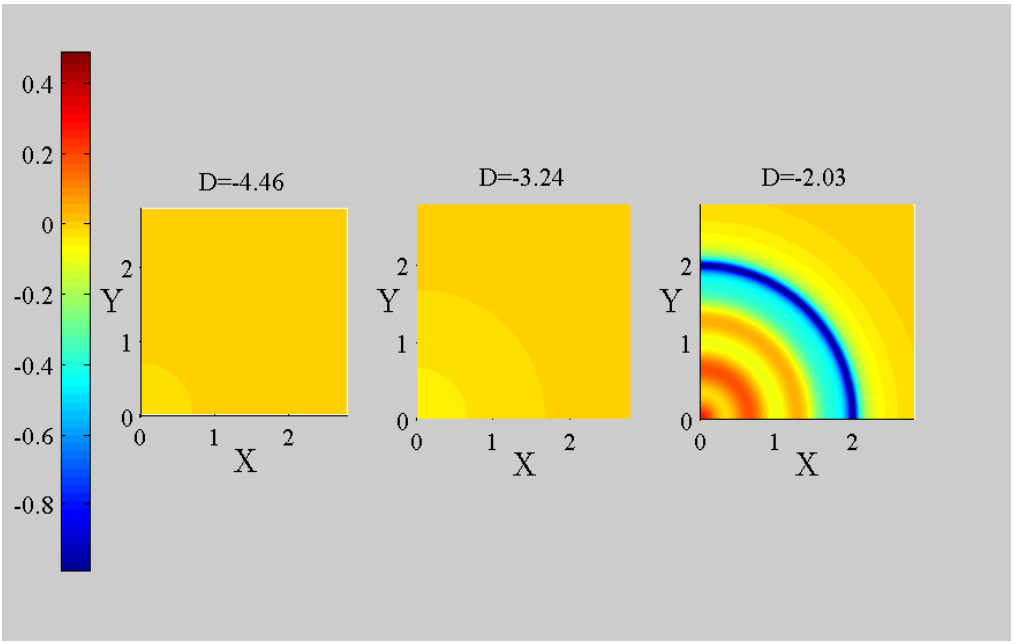

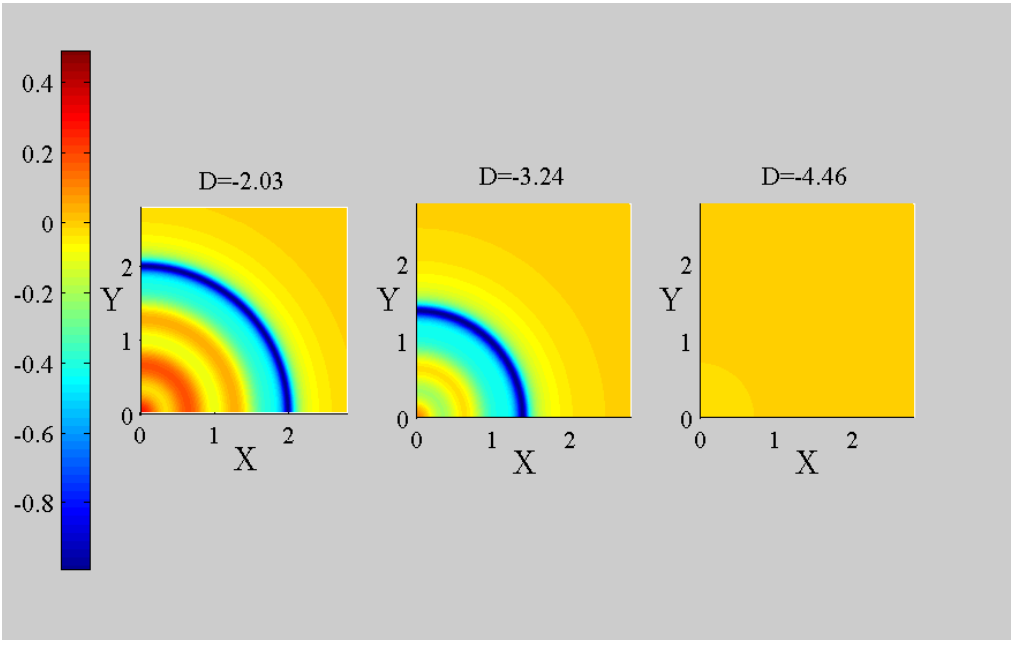

Figure A3

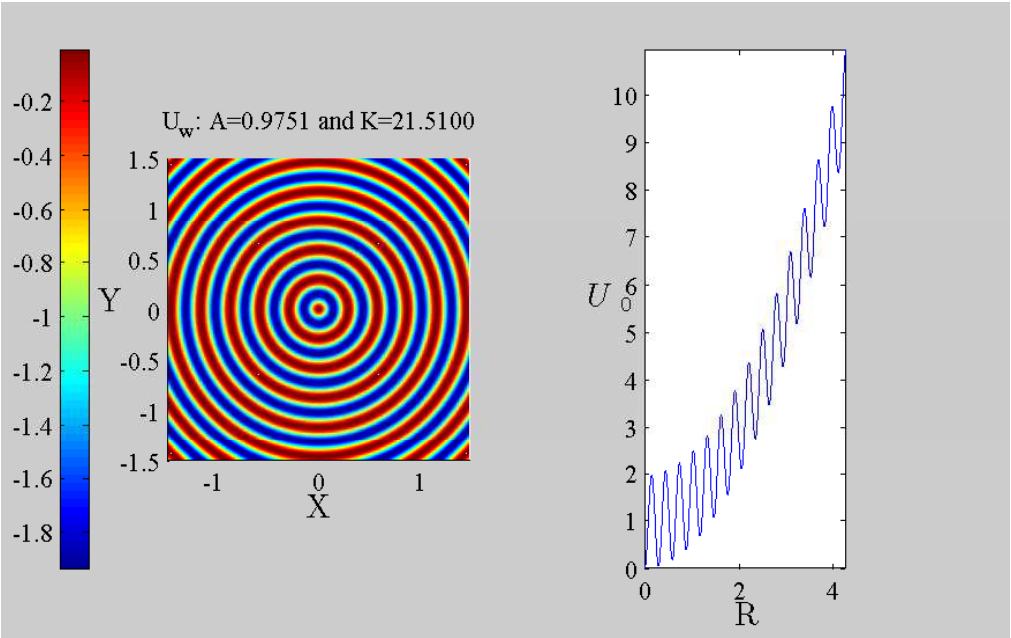

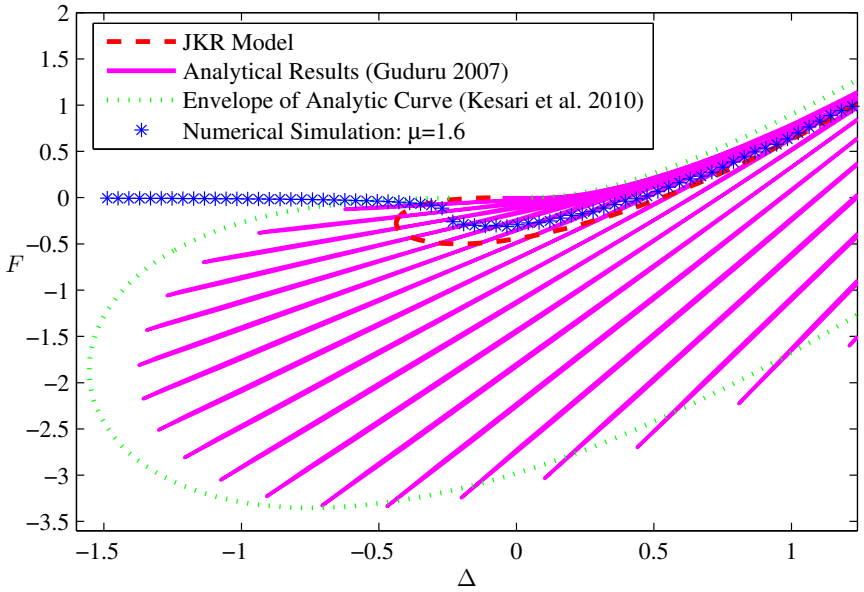

Figure A4

Experimental methods

Figures

B1. Schematic diagram of fabrication process of the rippled samples.

B2. Experimental setup for the indentation test. A spherical indenter is lowered into the sample to a certain depth and then pulled out using a motorized stage. The load on the indenter is measured using an in-line load cell and the area of contact between the indenter and sample is obtained by recording its image through the inverted optical microscope. The experiments are carried out using the same indentation and retraction rate.

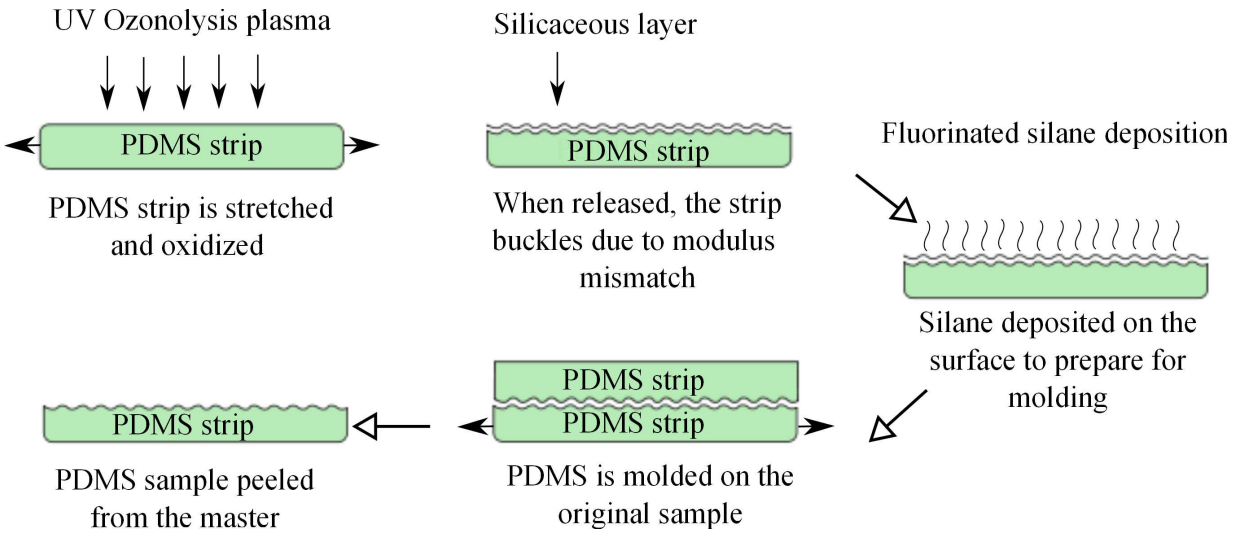

Figure B1

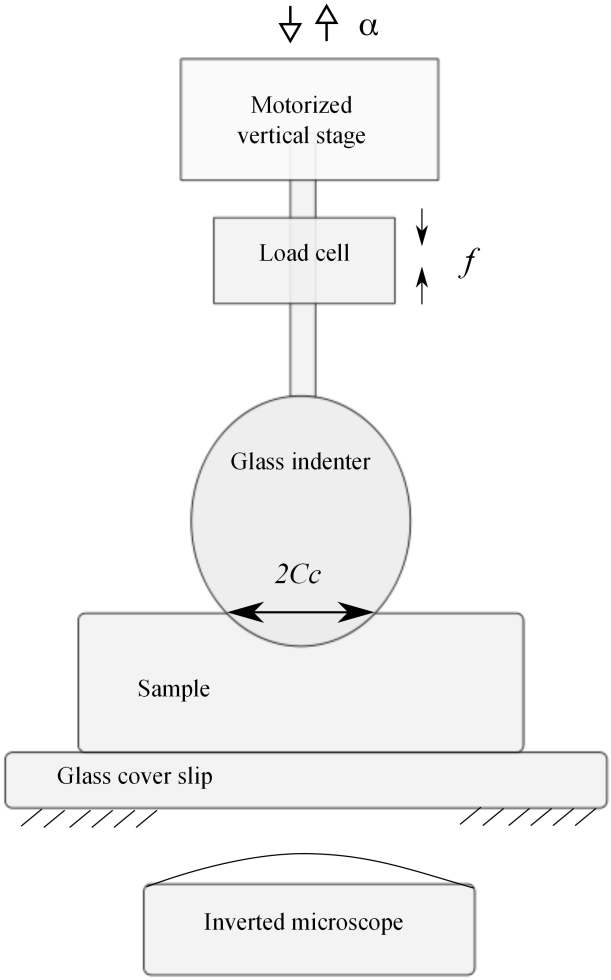

Figure B2